Korean J. Chem. Eng., 38(6), 1104-1116 (2021)
DOI: 10.1007/s11814-021-0741-4

pISSN: 0256-1115
eISSN: 1975-7220

INVITED REVIEW PAPER

A review of synthesis strategies for MOF-derived single atom catalysts

Jongkook Hwang†

Department of Chemical Engineering, Ajou University, Worldcupro 206, Suwon 16499, Korea
(*Received 10 November 2020 • Revised 31 December 2020 • Accepted 4 January 2021*)

Abstract−Single atom catalysts (SACs) have attracted great attention as promising catalysts that integrate the benefits of both heterogeneous and homogeneous catalysts. SACs exhibit unique properties that are otherwise difficult to achieve, such as high atom utilization efficiency, unprecedentedly high catalytic activity and selectivity. However, it still remains a great challenge to prepare stable SACs without particle aggregation and sintering. Among the various fabrication methods for SACs, metal-organic framework (MOF)-derived synthesis routes have shown great potential by taking advantage of MOFs' high structural/chemical tunability, large surface area and high porosity. In this review, the synthesis strategies for MOF-derived SACs are comprehensively summarized and classified into five classes, metal node modification, ligand modification, guest encapsulation, migration and trapping, and others. The current challenges and future opportunities of MOF-derived SACs are further discussed. This review will be useful for the rational design of MOF-derived SACs for various catalytic reactions.

Keywords: Single Atom Catalyst, Metal-organic Frameworks, Metal-organic Framework-derived Materials

INTRODUCTION

Currently, more than 95% of chemical products worldwide are manufactured by catalytic processes[1]. Catalysts play an essential role in increasing the reaction rate and selectivity for target chemicals under relatively mild conditions, reducing energy consumption and lowering operating costs. The total market size for industrial catalyst is estimated at $16 billion in 2015 [1]. Therefore, it is not difficult to understand why the development of economical and effective catalysts has been of particular research interest in chemistry, materials science and chemical engineering [2]. In general, the catalysts can be grouped into heterogeneous and homogeneous catalysts. Heterogeneous catalysts are typically comprised of catalytically-active metal particles and robust solid supports. They are widely used in industry due to their high stability and easy recyclability. However, only surface metal sites directly contribute to a reaction, while most of the metal atoms are buried in the bulk. For example, even 4 nm of metal nanoparticles (NPs) has a largely limited atom utilization efficiency of 20% with a significant fraction of unused bulk atoms [3]. In addition, traditional heterogeneous catalysts usually exhibit broad metal particle size distribution and poorly-defined irregular structure, which sometimes makes it difficult for researchers to understand the underlying reaction mechanism. Thus, it is natural that different research groups report several controversial results for the same catalysts. On the other hand, homogeneous catalysts have well-defined site-isolated metal centers with high metal atom utilization efficiency. Homogeneous catalysts usually show excellent catalytic activity and selectivity; however, the inherently low stability and poor recyclability have greatly limited their industrial use [1,4].

In recent years, single atom catalysts (SACs) have attracted significant attention as promising catalysts that integrate the advantages of heterogeneous and homogeneous catalysts, including high stability, easy separation and recycling, high selectivity and high atom utilization efficiency [3,5-9]. According to Zhang and coworkers, SACs are defined as a supported metal catalyst exclusively containing isolated monometallic active sites on a surface [10]. The particular advantages of SACs are as follows. i) SACs have atomically dispersed metal sites on the surface of solid supports, which maximizes the atom utilization efficiency close to 100% with a very high activity per unit mass. ii) The low-coordinated environment, fully exposed active sites, as well as the unique electronic structures of SACs greatly enhance the catalytic activity for various reactions (Fig. 1). iii) The single atom (SA) nature also contributes to enhancement of the product selectivity. SACs have uniform geometric configuration and active sites, making all reactants to have nearly the same spatial/electronic interaction with SACs, and thereby offering great potential to achieve high selectivity for target products [3,5-8]. In addition, because of the absence of ensemble sites where more than two atoms in the reactants are adsorbed together, SACs can follow the reaction pathway that is different from conventional metal NPs [11]. Thus, SACs can either suppress or promote the formation of certain product, providing new opportunities to control product selectivity. iv) The structural homogeneity of SACs facilitates the identification of the active sites and the fundamental understanding of structure-performance relationship at the atomic level.

Since the first practical preparation of single Pt atom catalysts by Zhang's group in 2011 [12], significant research efforts have been devoted to fabricating SACs with high catalytic activity, selectivity and stability [5-8,11,13-15], which are suitable for a variety of thermocatalytic [15,16], photocatalyic [17-19], and electrocatalytic

†To whom correspondence should be addressed.
E-mail: jongkook@ajou.ac.kr

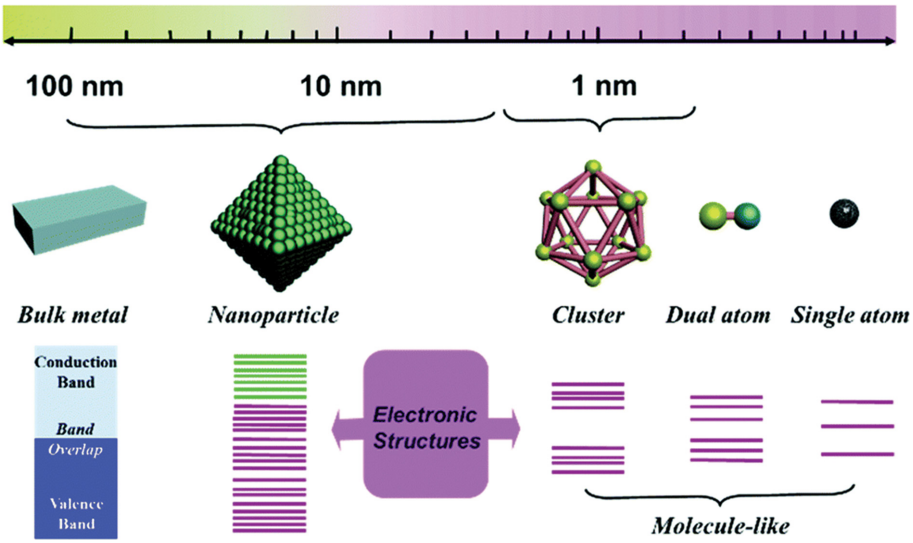

Fig. 1. Geometric and electronic structure of single/dual-atom, cluster and bulk metal materials (Reprinted with permission from Ref. [5], Copyright 2020, Royal Chemical Society).

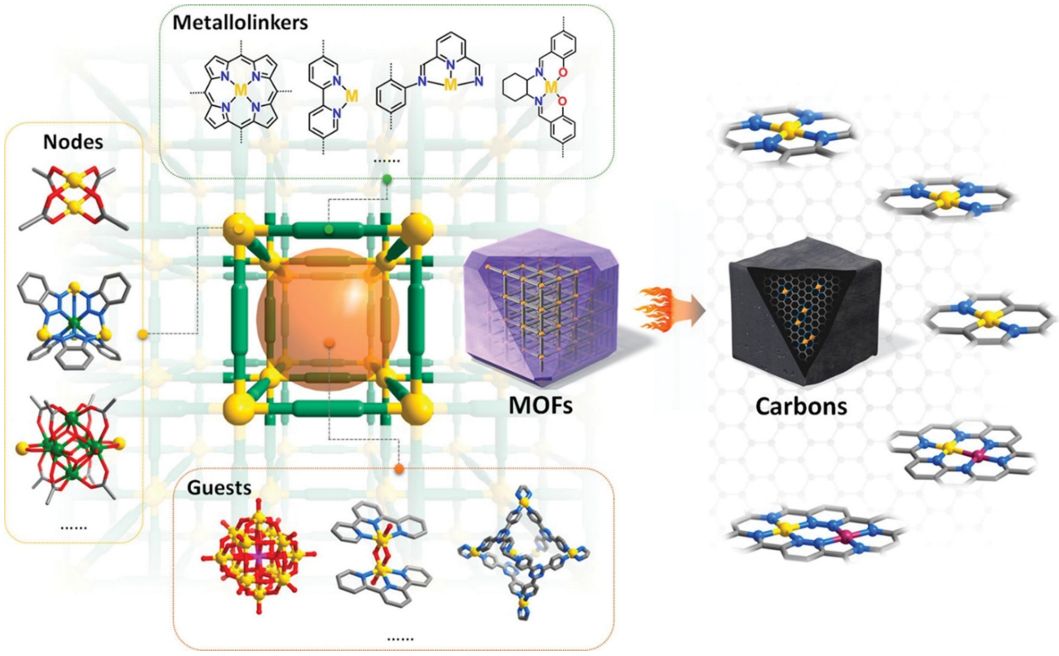

Fig. 2. Schematic illustration of various representative types of single metal-site catalysts based on MOFs and MOF-derived carbons. Color code: open metal sites, yellow; inactive metal cations, green; N, blue; O, red; C, gray (Reprinted with permission from Ref. [15], Copyright 2020, American Chemical Society).

applications [20-30]. Various approaches, including wet chemistry [12,31], atomic layer deposition [32], and gas-phase migration [33], have been reported so far. Among them, pyrolysis of metal-organic framework (MOF) has shown great promise in direct fabrication of SAC on carbon and other supports [13-15,17]. MOFs are an emerging class of crystalline porous materials constructed from inorganic metal nodes as secondary building units and a wide variety of organic ligands as linkers [34,35]. MOF are now believed to be versatile "all-in-one" precursors containing both inorganic metal nodes as source of metal species and organic linker as source of carbon and heteroatom. Thus, MOFs have been widely used as precursors/templates for preparation of a plethora of MOF-derived materials [36-43] and MOF-derived SACs [13-15,17].

MOF-derived synthesis of SACs has particular advantages over the other SAC preparation methods (Fig. 2). i) The unique structural characteristics of parent MOFs, such as high surface area, well-defined pore size and structures, and high chemical tunability, can be inherited to daughter MOF-derived SACs, increasing the mass transport capability and the accessibility to active SA sites. ii) Since the metal nodes of MOFs are atomically and homogeneously dis-

tributed within the framework's well-defined coordination environment, pristine MOF itself can be directly converted to SACs through a simple one-step pyrolysis. iii) In addition, by taking advantage of MOF's structural tunability, metal nodes and organic linkers can be post-modified to anchor/stabilize the metal atoms. iv) Various guest species, such as metal salts, metal complex, and NPs, can be further accommodated in the uniform pores of MOFs. These features make MOF an ideal precursor/template for construction of SACs.

Although there are several reviews on SACs [3,6,8-10,44-48], a systematic discussion of the preparation of MOF-derived SACs is still insufficient. In this review, we comprehensively summarize the synthesis strategies for MOF-derived SACs. We categorized the synthesis strategies into five groups, depending on the formation mechanism of SA metal sites on the support. Inorganic metal nodes are either used as sources for SACs or modified to include additional

Table 1. Summary of MOF-derived SACs

Synthesis strategies	Parent precursor	Metal sites	Metal content (wt%)	Application	Ref.
Metal node modification (MNM)	Zn/Co-ZIF	Co-N_x	4.0	ORR	[49]
	Zn/Co-ZIF	Co-N_x	1.7	ORR	[50]
	Zn/Co-ZIF	Co-N_x	0.34	ORR	[51]
	Zn/Co-ZIF	Co-N_x	0.25	CO_2RR	[52]
	Zn/Fe-ZIF	Fe-N_x	0.45	ORR	[53]
	Zn/Fe-ZIF	Fe-N_x	0.15	ORR	[54]
	Zn/Ni-ZIF	Ni-N_x	5.44	CO_2RR	[55]
	Zn/Ni-ZIF	Ni-N_x	N/A	Hydrogenation of acetylene	[56]
	MgNi-MOF-74	Ni-N_x	0.9	CO_2RR	[57]
	Mn-BTC	Mn-N_x	0.23	ORR	[58]
	ZIF-8	Zn-N_x	11.3	CO_2 cycloaddition	[59]
	ZIF-8	Zn-N_x	3.12	Peroxidase mimic	[60]
Ligand modification (LM)	PCN-222 (mixed ligand)	Fe-N_x	1.76	ORR	[61]
	UiO(bpdc)-$FeCl_3$	Fe-N_x	1.5	ORR	[62]
	ZIF-8@Ammonium ferric citrate	Fe-N_x			[63]
	UiO-66-NH_2-Pd^{2+}	Pd_1/ZrO_2	0.44	Indole synthesis	[64]
	UiO-66-NH_2-Ru^{4+}	Ru-N_x	0.3	Hydrogenation of quinoline	[65]
	UiO-66-NH_2-W^{6+}	W-N_x	1.21	HER	[66]
Guest encapsulation (GE)	$Fe(acac)_3$@ZIF-8	Fe-N_x	2.16	ORR	[67]
	FePc@ZIF-8	Fe-N_x	0.20	ORR	[68]
	$FePc(CN)_8$@ZIF-8	Fe-N_x	2.0	ORR	[69]
	ferrocene@ZIF-8	Fe-N_x	0.43	ORR	[70]
	$FeCl_3$@MIL-101-NH_2	Fe-N_x	1.1	ORR	[71]
	Fe-mIm@ZIF-8	Fe-N_x	5	ORR	[72]
	$CrCl_3$@ZIF-8	Cr-N_x	0.62	ORR	[73]
	$Ir(acac)_3$@ZIF-8	Ir-N_x	0.20	ORR	[74]
	$Ru(acac)_3$@ZIF-8	Ru-N_x	0.18	N_2RR	[75]
Migration trapping (MT)	Bi-MOF derived Bi NPs@NC	Bi-N_x	0.2	CO_2RR	[76]
	Bulk Cu foam and ZIF-8	Cu-N_x	0.54	ORR	[77]
	Bulk Cu_2O and ZIF-8	Cu-N_x	0.45	ORR	[78]
	Bulk Fe_2O_3 and ZIF-8	Fe-N_x	1.2	Fenton catalysis	[79]
	Ferrocene and ZIF-8	Fe-N_x	1.0	ORR	[80]
	Ni/ZIF-8 derived Ni NPs@NC	Ni-N_x	NA	CO_2RR	[81]
	Pd NPs@ZIF-8	Pd-N_x	0.16	Hydrogenation of acetylene	[82]
Others	Zn/Co-ZIF@F127, polymer coating	Co-N_x	0.9	ORR	[83]
	Fe-doped ZIF-8@PZS polymer coating	Fe-N_x	1.54	ORR	[84]
	SiO_2@PCN-222(Fe)	Fe-N_x	3.46	ORR	[85]
	Mn-ZIF-8 derived Mn-NC, two-step adsorption and pyrolysis	Mn-N_x	3.03	ORR	[86]
	SiO_2@NU-1000, silica nanocasting	Zr_6@SiO_2	23	Glucose isomerization	[87]

secondary metal species in the frameworks (metal node modification (MNM), Section 2.1). The target metal species are introduced to the ligand (ligand modification (LM), Section 2.2) or confined within the pores of MOFs (guest encapsulation (GE), Section 2.3). The metal NPs and bulk metals can also be converted to SA through thermal migration and trapping (migration trapping (MT), Section 2.4). Finally, several synthesis methods that do not fall into the preceding four categories will be summarized (Section 2.5).

SYNTHESIS STRATEGIES FOR MOF-DERIVED SACs

The synthesis strategies of MOF-derived SACs and their applications are comprehensively summarized in Table 1. Compared to MOF-supported SACs, MOF-derived SACs have high thermal and chemical stability as well as excellent electrical conductivity, making them suitable for various catalytic processes. Indeed, a wide range of MOF-derived SACs with diverse single metal sites and metal configurations have been fabricated and utilized for a number of thermocatalytic reactions (*e.g.*, CO_2 cycloaddition, hydrogenation of acetylene) [15,16] and electrocatalytic reactions (oxygen reduction reaction, (ORR), nitrogen reduction reaction (NRR), and CO_2 reduction (CO_2RR) [20-28] (Table 1).

1. Metal Node Modification

The use of metal nodes as a sole source of SA is a simple and straightforward strategy toward MOF-derived SACs because the metal nodes (metal ions) are inherently atomically dispersed within MOFs. The metal node can be used as is or can be further replaced with external secondary metal ions. Yang et al. found that direct pyrolysis of hollow zeolitic imidazole frameworks-8 (ZIF-8) led to fabrication of ultrahigh Zn atoms (11.3 wt%) supported on N-doped hollow carbons [59]. Nitrogen-rich ligands (2-methylimidazole ligand) converted to carbon matrix with abundant nitrogen

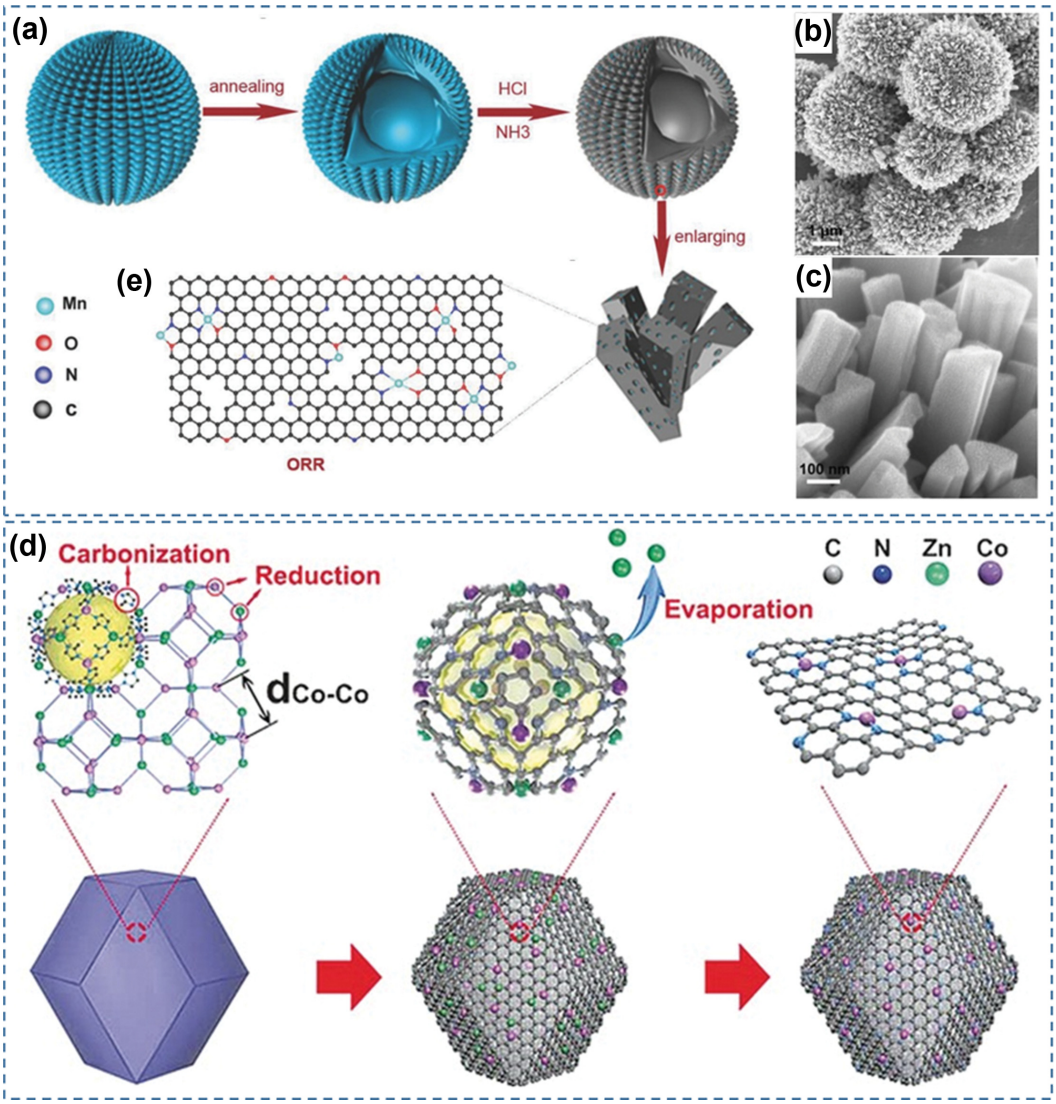

Fig. 3. Metal node modification. (a) Schematic illustration of the synthetic process for Mn/C-NO and their field emission scanning electron microscopy (SEM) images with different magnification ((b), (c)), (Reprinted with permission from Ref. [58], Copyright 2018, John Wiley & Sons), (d) The formation of Co SAs/NC *via* pyrolysis of bimetallic Zn/Co ZIFs with controlled Zn/Co molar ratios (Reprinted with permission from Ref. [49], Copyright 2016, John Wiley & Sons).

coordination sites effectively stabilize the isolated Zn metal atoms through Zn-N_4 coordination. Xu et al. reported that ZIF-8 derived Zn-N_x SACs have unique peroxidase-like behavior, showing great promise for wound antibacterial applications [60]. While direct pyrolysis can be used for formation of SACs, it often requires additional acid etching and activation steps that are tedious and time-consuming. Chen and coworkers reported preparation of 3D graphene supported manganese (Mn) SAC through direct pyrolysis of Mn-BTC MOF under nitrogen gas atmosphere, followed by HCl etching and NH_3 activation [58] (Fig. 3(a)-(c)). Acid etching step was required to eliminate the aggregated metal NPs, leaving the stabilized SAs on the carbon support. NH_3 activation ensured the formation of Mn atoms coordinated with N and O atoms embedded in 3D graphene. Similarly, Ni-SA catalysts were also synthesized by direct pyrolysis of Ni-MOF, followed by acid etching and electrochemical activation [88]. However, severe particle sintering and aggregation largely restrict the applicability of the direct pyrolysis approach.

These limitations can be alleviated by using predesigned MOF with mixed metal ions and abundant metal-coordination functionalities. Secondary metal ion can be implanted into the metal node of MOF through direct formation of mixed-metal MOFs or post-synthetic ion exchange. This mixed-MNM strategy can spatially separate the target metal ions with extended adjacent distances, minimizing the undesired metal aggregation during pyrolysis. In addition, it can finely control the amount of target metal in the frameworks to maximize the M-N coordination sites. Pyrolysis of mixed-metal ZIFs has been widely used in fabrication of SACs. [49-52,89]. Jiang and coworkers reported this strategy for the first time in 2015 [89]. Since Zn^{2+} and Co^{2+} have similar ionic sizes and coordination types with 2-methylimidazole ligand, Zn/Co bimetallic ZIF with uniform distribution of Zn and Co ions were directly prepared. Upon pyrolysis, Zn metal (boiling point of 906 °C) was selectively removed by evaporation along N_2 gas flow, leaving the isolated Co atom coordinated with nitrogen-doped carbon support (Co-NC SACs). In a similar manner, Yin et al. prepared single cobalt atoms with high Co loading (4 wt%) and precise N-coordination (Co-N_4, Co-N_3, Co-N_2 configuration) (Fig. 3(d)) [49]. The added Zn^{2+} replaced a certain proportion of Co^{2+} sites in metal nodes and act as a fence that further extends the adjacent distance of Co atoms (Fig. 3(d)). Adjusting the molar ratio of Zn/Co to above 1 increases the distance of adjacent Co atoms and provides more free N sites that stabilize Co atoms without forming Co NPs [50]. Instead of ZIFs, bimetallic MOF-74 could be also utilized for the preparation of various SACs. Gong et al. prepared polypyrrole (PPy)-encapsulated-MgNi-MOF-74 and utilized it as a precursor for Ni-SA/NC catalysts for electrochemical CO_2 reduction reaction [57]. A large amount of Mg^{2+} extends the distance between adjacent Ni atoms while PPy served as source of N atoms which anchor/stabilize the Ni SAs (0.9 wt%). The Mg species were converted to aggregated MgO nanoparticles that are removed by acid etching. Ni SA/NC catalysts with controlled Ni-N coordination number as well as other types of SACs, such as Co and Fe SACs were successfully fabricated.

Different from Co^{2+}, most of the other metal ions cannot directly form bimetallic ZIF with Zn^{2+}. To circumvent this problem, post-synthetic ion exchange/doping has been applied to partially replace the Zn to Cu [90], Fe [53,54,91-93], Ni [55-57,94]. The predesigned mixed-metal MOFs have allowed preparation of Cu, Fe, and Ni SA supported carbon catalysts *via* direct one-step pyrolysis. For example, Zhao et al. reported ion exchange between Zn nodes and adsorbed Ni ions within the cavities of the ZIF-8 to access single nickel sites for efficient electroreduction of CO_2 [94]. In another case, Shui and coworkers developed a sequential coordination method to dope precious metal ions into ZIF and prepared Ir, Rh, Pt, and Pd SA/NC catalysts with metal loading as high as 1.2-4.5 wt% [95].

2. Ligand Modification

A wide variety of organic linkers with different chemical composition and functional groups have been utilized in MOF synthesis without changing the original crystal structure and topology. These features make organic linkers as versatile anchoring sites for metal atoms, offering new opportunities for construction of MOF-derived SACs. In particular, amino functionalized ligands [65] and porphyrin-based ligands [61] have been most popularly adopted to coordinate the target metal atoms. Wang et al. utilized free amine groups at the linker of UiO-66-NH_2 as coordination sites for Ru^{3+} cations to gain isolated atomic dispersion of Ru on NC materials (Fig. 4(a)). During pyrolysis at 700 °C under argon atmosphere, Zr metal nodes of MOF converted to ZrO_2 which is removed by HF etching, leaving highly porous carbon structures. Meanwhile, Ru^{3+} ions were carbothermally reduced to Ru metal atoms [65]. This strategy was further extended to prepare tungsten SACs (W-NC) for electrochemical hydrogen evolution revolution [66]. In addition, Wu and coworkers reported fabrication of Pd SA on 3D ZrO_2 *via* two-step carbothermal welding strategy [64]. Pd^{2+} anchored UiO-66-NH_2 was first transformed to Pd@NC/ZrO_2 during pyrolysis under Ar atmosphere. Subsequent gas switching from Ar to air led to selective combustion of carbon species and formation of rigid ZrO_2 nano-networks, leaving a sinter-resistant Pd_1@ZrO_2 catalyst *via* atom trapping. Lin et al. prepared a series of SAC through post-synthetic modification of bipyridine sites of UiO(bpdc) MOF [62]. The bipyridine provided two active N sites located at the backbone of the framework, which can chelate transition metal ions homogeneously (Fig. 4(b)). The resulting UiO(bpdc)-M_xCl_y (M=Fe, Co, Ni and Cu) subsequently underwent pyrolysis and acid etching, and transformed to SAC/NC with unique M-N_5 configuration. As an alternative pathway, post-synthetic ligand exchange has been proposed by Bao and coworkers to prepare highly exposed Fe-N sites catalysts for ORR. When ammonium ferric citrate was added to the dispersion of preformed ZIF-8 aqueous solution, surface-exposed 2-methylimidazole ligands were exchanged with citrate ions. The citrate ion is too bulky to penetrate into the inner space of ZIF-8, so it anchors Fe atoms only onto the surface of ZIF-8, leading to formation of surface-enriched atomic Fe-N sites after pyrolysis [63].

A mixed-ligand strategy employing metalated and metal-free ligands can offer a novel pathway to control the distance of adjacent metal sites, in a manner similar to the mixed-metal strategy described in Section 2.1. A mixed-ligand strategy can enlarge the distance between metal atoms, facilitating the formation of SAC without particle sintering during high temperature pyrolysis. Jiang and coworkers simultaneously utilized TCPP (tetrakis (4-carboxy-

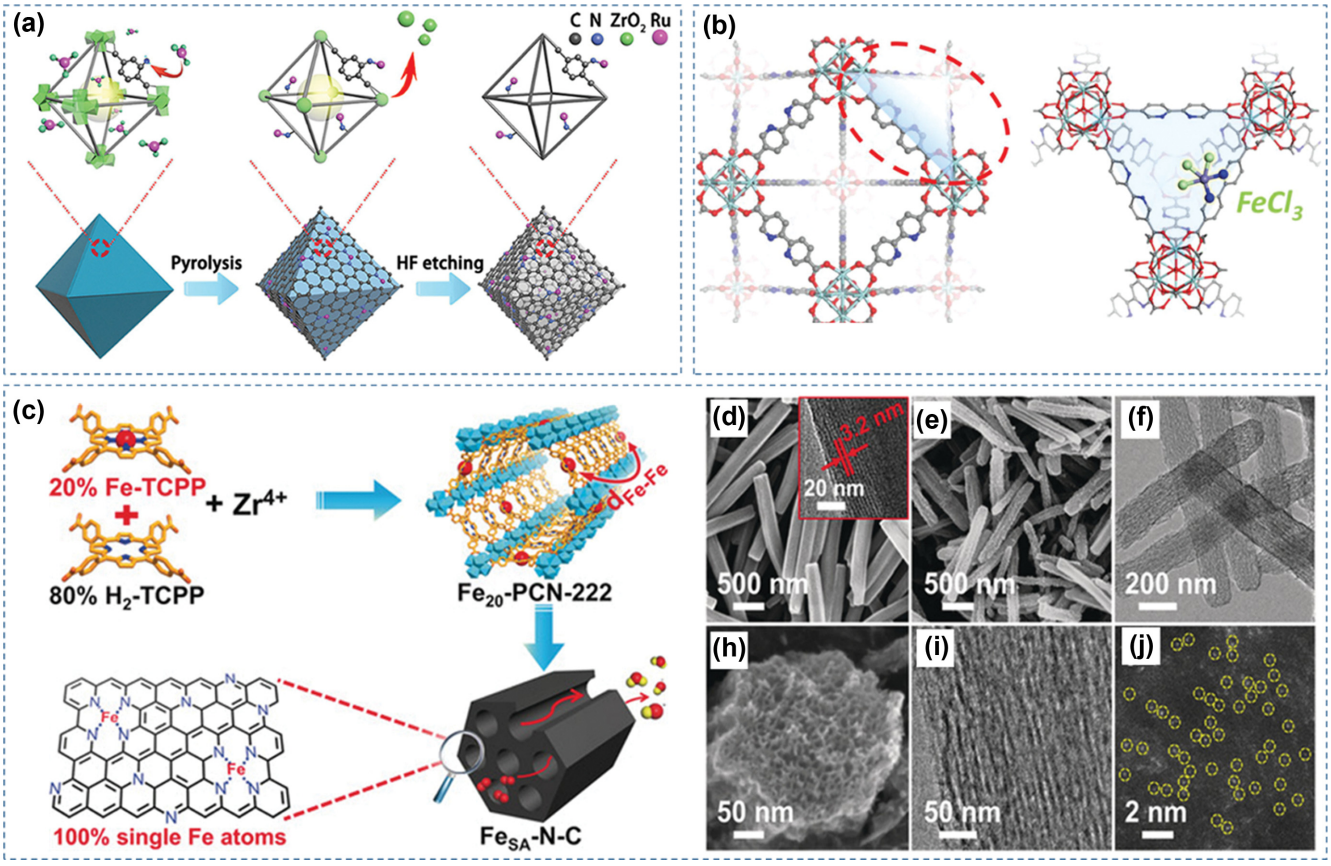

Fig. 4. Ligand modification. (a) Schematic illustration of the synthetic process for Ru SAs/NC from UiO-66-NH_2/Ru^{2+}, (Reprinted with permission from Ref. [65], Copyright 2017, American Chemical Society), (b) Anchoring N-sites in bipyridine ligand of UiO(bpdc) and UiO(bpdc)-$FeCl_3$, (Reprinted with permission from Ref. [62], Copyright 2019, John Wiley & Sons), (c) Schematic illustration of Fe SA/NC catalyst *via* a mixed-ligand strategy, (d)-(h) SEM image, (i) transmission electron microscopy (TEM) image and (j) high-angle annular dark-field scanning transmission electron microscope (HAADF-STEM) image of Fe SA/NC, (Reprinted with permission from Ref. [61], Copyright 2018, John Wiley & Sons).

phenyl)porphyrin) ligand with and without Fe(III) centers (H_2-TCPP and Fe-TCPP, respectively) to prepare a series of isostructural porphyrinic PCN-222 MOF (Fig. 4(c)) [61]. When optimum amount of Fe-TCPP (20 mol%) was used, all Fe species were converted to atomically dispersed Fe atoms with high loading of 1.76% through simple one-step pyrolysis without additional acid etching process. Further increase of Fe-TCPP>20 mol% (*i.e.*, decrease of Fe-Fe distance) resulted in Fe atom aggregation to Fe NPs. The uniform rod morphology and highly ordered mesopores (3.2 nm) of parent Fe-PCN-222 were well-inherited to derived Fe SACs (Fig. 4(d)-(i)).

3. Guest Encapsulation

Benefiting from highly ordered and controllable pore size and pore structures, MOFs can serve as effective host materials that accommodate diverse guest metal species (namely, guest encapsulation or host-guest approach). The guest species must be confined and isolated in the hosts to prevent their aggregation into large particles and escaping from the MOF pores. To this end, the molecular size of metal precursors need to be greater than half the pore size of the MOFs but smaller than the pores of the MOFs, so that only one guest molecule is confined in one pore of the MOFs. In general, guest metal precursors are encapsulated through either *in situ* crystallization or post-synthetic confinement (Fig. 5). Chen et al. simply added guest iron acetylacetonate ($Fe(acac)_3$, molecular diameter of 9.7 Å) to the conventional ZIF-8 synthesis solution (Fig. 5(a)) [67]. The coordination of Zn^{2+} and 2-methylimidazole forms cages with cavity diameter of 11.6 Å and pore diameter of 3.4 Å, which enables the isolation and encapsulation of one Fe molecule in one cage. Pyrolysis at 900 °C led to transformation of $Fe(acac)_3$@ZIF-8 to isolated Fe atoms anchored on NC (Fe-ISA/NC) (Fig. 5(a)). Fe loading was controlled up to 2.16 wt% by simply changing the amount of $Fe(acac)_3$ used. Inspired by this contribution, researchers have successfully used other metal acetylacetonates such as $Ir(acac)_3$ [74], $Ru(acac)_3$ [75,96], $Rh(acac)_3$ [97] to fabricate corresponding SACs. In a similar manner, metal salts and metal complex are directly confined within the cages of MOF during MOF crystallization. Yin and coworkers fabricated Fe SA embedded NC using ferrocene with a molecular size of 6.4 Å [70]. The use of iron phthalocyanine (FePc) with a molecular size of 14.6 Å, which is larger than the size of ZIF's cage, broke the confinement effect of cages, thereby leading to generation of the mixture of Fe SAs (0.20 wt%) and Fe_2O_3 NPs [68]. To facilitate the

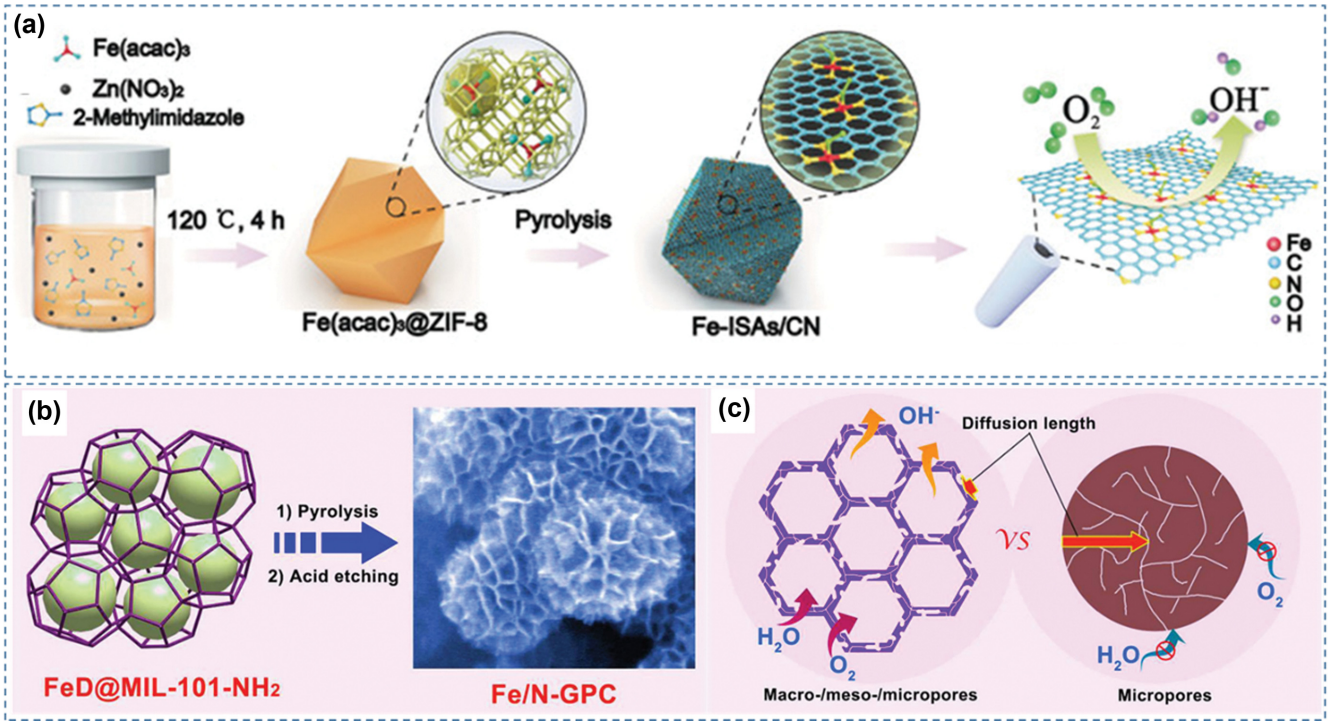

Fig. 5. Guest encapsulation. (a) Schematic illustration of the formation of Fe-ISAs/NC through pyrolysis of *in situ* crystallized Fe(acac)$_3$@ZIF-8, (Reprinted with permission from Ref. [67], Copyright 2017, John Wiley & Sons), (b) Schematic illustration of the preparation of the Fe/N-GPC catalyst through post-synthetic encapsulation, and (c) advantages of the hierarchically porous architecture of Fe/N-GPC in ORR, (Reprinted with permission from Ref. [71], Copyright 2017, American Chemical Society).

incorporation of FePc and the formation of Fe SA sites, Wang et al. used octacyano substituted FePc(CN)$_8$ as an iron precursor [69]. Cyano groups promote the incorporation of FePc molecules into ZIF-8 due to the coordination between the cyano group and the Zn ion, resulting in a higher iron loading (up to 2.60 wt%) and more Fe-N$_x$ active sites than their FePc counterparts. In another report, a pre-synthesized Fe-phen (1,10-phenanthroline) complex [98] and Fe-mIm nanocluster [72] were employed as guest species. In addition, Xing and coworkers synthesized Cr-NC SACs by absorption of $CrCl_3 \cdot 6H_2O$ into the pores of ZIF through host-guest interactions, followed by pyrolysis and acid leaching of excess Cr species [73].

Post-synthetic confinement is another promising way to expand the range of possible metal precursors used for MOF-encapsulation. This strategy is particularly attractive when the direct encapsulation *via in situ* crystallization is difficult or impractical. Post-synthetic encapsulation was achieved by using the double solvent method which has been previously employed for the confinement of metal NPs into the pores of MOFs [99,100]. MIL-101-NH$_2$, with high surface area, large pore size (2-3 nm) and hydrophilic pore environment, was chosen as a host to accommodate dicyandiamide (N source) and $FeCl_3$ (Fe source) [71]. Dicyandiamide and $FeCl_3$ dissolved in hydrophilic dimethylformamide (DMF) was added to a hydrophobic *n*-hexane suspension of MIL-101-NH$_2$. The dispersed hydrophilic droplets diffused into the hydrophilic pores of MOFs completely, allowing selective encapsulation of nitrogen and Fe precursors into the pores of MOFs (Fig. 5(b)). The resulting Fe-NC catalysts showed high catalytic performance for ORR due to unique hierarchically porous macro-meso-microporous structures and uniformly distributed Fe-N SA sites (Fig. 5(c)).

4. Migration Trapping

During high temperature pyrolysis, supported metal NPs often sinter to large particles *via* Ostwald ripening mechanism [101,102]. The mobile species are emitted from smaller particles and transported to nearby larger particles because of their different surface energies, *i.e.*, the larger particles grow at the expense of the smaller particles. However, from a different point of view, the conditions under which the NPs release mobile species can be utilized to create atomically dispersed SACs if the mobile species can be effectively trapped and captured by the support. In 2016, Datye and coworkers pioneered this MT strategy for preparation of thermally stable Pt SA on ceria catalysts. When the physical mixture of Pt/Al_2O_3 and CeO_2 was aged in flowing air at 800 °C, Pt was emitted as volatile PtO_2 and completely migrated to the CeO_2 which traps atomically dispersed Pt species. The key to the success of this strategy is the emission of mobile species from metal NPs (bulk metal) and their capture by support through strong-metal support interaction (SMSI). It was found that MOF-derived NC is able to trap mobile metals by forming metal-N bonds. Indeed, Li and coworkers reported the transformation of noble metal NPs (Pd, Pt, Au NPs to thermally stable SAs (Pd, Pt, Au-SAs) above 900 °C in an inert atmosphere [82]. They investigated the NP-to-SA transformation process with *in situ* environmental TEM and density functional theory (DFT) calculations. It was revealed that sintering played a major role at relatively low temperature (300-900 °C) while atomization dominated at high temperature (900-1,000 °C). Since the Pd-

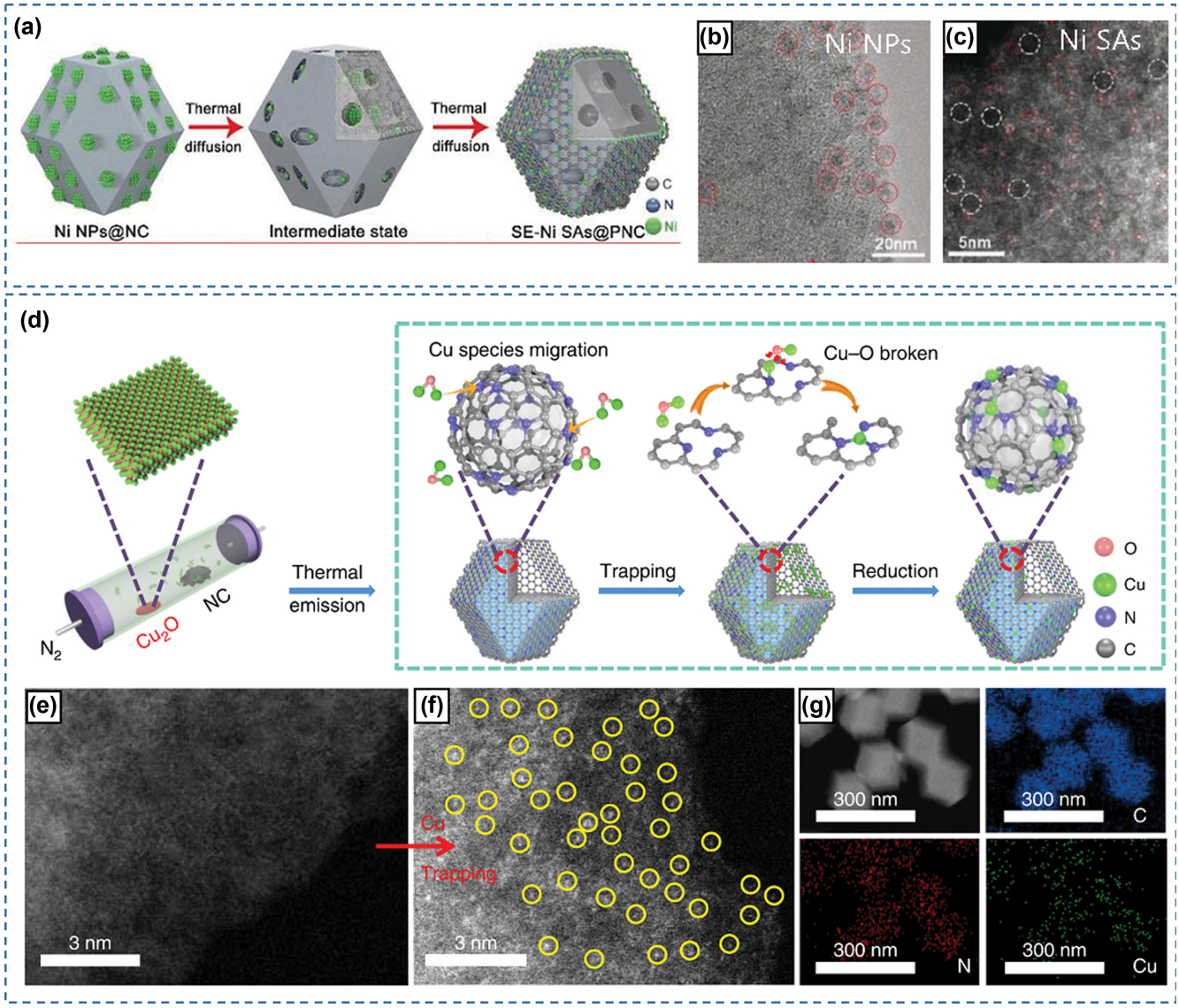

Fig. 6. Migration trapping. (a) Schematic illustration of the thermal *in situ* transformation of Ni NPs to Ni SAs, TEM image of (b) Ni NPs@NC and (c) Ni SAs@PNC (Reprinted with permission from Ref. [81], Copyright 2018, John Wiley & Sons), (d) Schematic illustration of direct transformation of bulk Cu_2O into Cu-SAs/NC *via* emitting and trapping of atoms, (Licensed under CC-BY from [78]), (e) aberration-corrected high-angle annular dark-field scanning transmission electron microscope (AC HAADF-STEM) image of NC, (f) AC HAADF-STEM image of Cu ISAS/NC, (g) corresponding energy dispersive x-ray spectroscopy mapping of Cu ISAS/NC.

N_4 bonds are thermodynamically more stable than Pd-Pd bonds, the formation of Pd-N_4 can act as a driving force for atomization. In a similar manner, Wu and coworkers reported the conversion of Ni NPs to the surface enriched Ni SAs on the NC support through thermal atomization (Fig. 6(a)-(c)) [81].

In recent years, Li and coworkers have opened up new possibilities for scalable production of functional SACs at the industrial level by directly manufacturing SACs from cost-effective bulk metals. They demonstrated the transformation of "bulk" Cu metal into Cu SA *via* migration and atom trapping [77]. Atoms released from bulk metals are transported and trapped on NC with the assistance of NH_3 gas. First, NH_3 gas carried the exposed Cu atoms out of Cu foam (bulk Cu source) and generated volatile $Cu(NH_3)_x$ species by the strong Lewis acid-base interaction. After that, the $Cu(NH_3)_x$ species were transported along the NH_3 gas stream and trapped at the defect sites in the ZIF-8 derived NCs, creating Cu-SAs/NC catalysts. This strategy is highly versatile and applicable to other bulk metals (Co, Ni, Pt) and support (graphene) for fabrication of SACs [77,103]. Instead of using NH_3 gas stream, *in situ* generated NH_3 from pyrolysis of dicyandiamide can be used to prepare Pt SACs [103]. Similarly, Zhang et al. reported fabrication of Bi-N_4 sites on porous carbon through pyrolysis of bismuth-MOF and dicyandiamide [76]. However, NH_3 molecules are toxic and corrosive, limiting the widespread utilization of this approach. To circumvent this problem, Wu and coworkers developed a versatile method that uses an inert N_2 gas flow and an inexpensive, readily available bulk metal oxide as a precursor, greatly expanding the applicability of the MT strategy (Fig. 6(d)-(g)) [78]. It was

found that bulk metal oxides (Cu_2O, MoO_3 and SnO_2) can be sublimated as mobile vapor at near their melting temperature, which are transported and trapped into defective N-rich carbon to form M-SA/NC catalysts (M=Cu, Mo, Sn). Likewise, the migration and trapping of Fe_2O_3 [79] and ferrocene precursors [80] to ZIF-8 derived NC were demonstrated to fabricate Fe SAs-NC catalysts. Very recently, Jia and coworkers unraveled how typical iron precursors (iron salts, Fe-doped ZIF-8) transform to single-atomic Fe-N_4 sites during pyrolysis *via* in-temperature X-ray absorption spectroscopy [104]. They revealed that Fe precursor transforms to Fe oxides below 300 °C and then to tetrahedral Fe_1(II)-O_4 below 600 °C. Above 600 °C, Fe_1(II)-O_4 releases a volatile single Fe atom, which diffuses to the defects of NC forming ORR-active Fe-N_4 sites. These results not only reveal the presence of gas-phase iron species during the high temperature pyrolysis process, but also provide a deeper understanding of SAC synthesis through the MT strategy.

5. Other Strategies

There are several approaches that do not exactly fall into the aforementioned four categories, such as ball-milling assisted strategy [106] and two-step adsorption and pyrolysis strategy [86,105]. Jaouen and coworkers fabricated a wide range of M-NC catalysts (M=Mn, Fe, Co, Ni and Cu) for electrocatalytic CO_2 reduction *via* dry ball-milling of ZIF-8, metal acetate, and 1,10-phenanthroline, followed by pyrolysis at 1,050 °C under Ar [106]. Instead of the direct pyrolysis of MOFs, the pre-synthesized MOF-derived carbon itself could be used as a versatile support that stabilizes the metal SA [86,105]. The adsorption-pyrolysis strategy uses MOF-derived carbon as a host to adsorb additional metal and nitrogen precursors, followed by a secondary thermal treatment (Fig. 7(a)). This process promotes the formation of SACs enriched at the surface of carbon support, increasing the accessibility to active SA sites. Li and coworkers soaked the ZIF-8 derived NC to metal salt-containing methanol solution for 24 h to adsorb $Fe(acac)_3$ or $Co(acac)_3$ [105]. Subsequent drying and pyrolysis at 900 °C under Ar led to formation of M-SA/NC catalysts with relatively low content of Fe (0.964 wt%) and Co (0.218 wt%). Wu and coworkers developed two-step adsorption-pyrolysis strategy to increase the density of atomically dispersed Mn-N_4 sites [86]. First, Mn-doped ZIF-8 was carbonized at 1,100 °C and acid-washed to prepare N-doped graphitic carbon host with a low density of Mn (0.68 wt%). Next, additional Mn and N sources were adsorbed into the preformed Mn-NC host and then carbonized again to generate increased density of Mn SAs (3.03 wt%). The resulting Mn-NC catalyst exhibited encouraging performance as a Pt-group metal free cathode in proton-exchange membrane fuel cells.

The preceding four strategies (in Section 2) are often combined with the sacrificial templates (tellurium nanotubes [107] and cadmium [108]), the top-down processing techniques (electrospinning [109]), and the protection by polymer [83,84] and SiO_2 [85,87, 110,111], to further suppress the particle migration and sintering and to achieve large surface area and high porosity. In particular, polymer-assisted MOF-pyrolysis (*e.g.*, polypyrrole, polythiophen, polydopamine, and F127) [57,112-114] has shown great promise to prepare MOF-derived SACs with high metal density and catalytic activity. Polymers have played important roles in controlling the size, structure, stability and processability of various inorganic materials [115-122] and MOFs [123-127]. Wu and coworkers coated the poly(cyclotriphospazeneco-4,4′-sulfonyldiphenol) (PZS) on the surface of bimetallic Fe-doped ZIF-8 (Fe/ZIF-8@PZS), to fabricate a Fe SAs (1.54 wt%) supported on a nitrogen, phosphorus and sulfur co-doped hollow carbon polyhedron (Fe-SAs/NPS-HC) (Fig. 7(b)) [84]. The polymer coating contributes to the improvement of kinetics and activity of the ORR by allowing the construction of a hollow structure through Kirkendall effect and modulation of electronic structures of an active metal center through N, P, S co-doping.

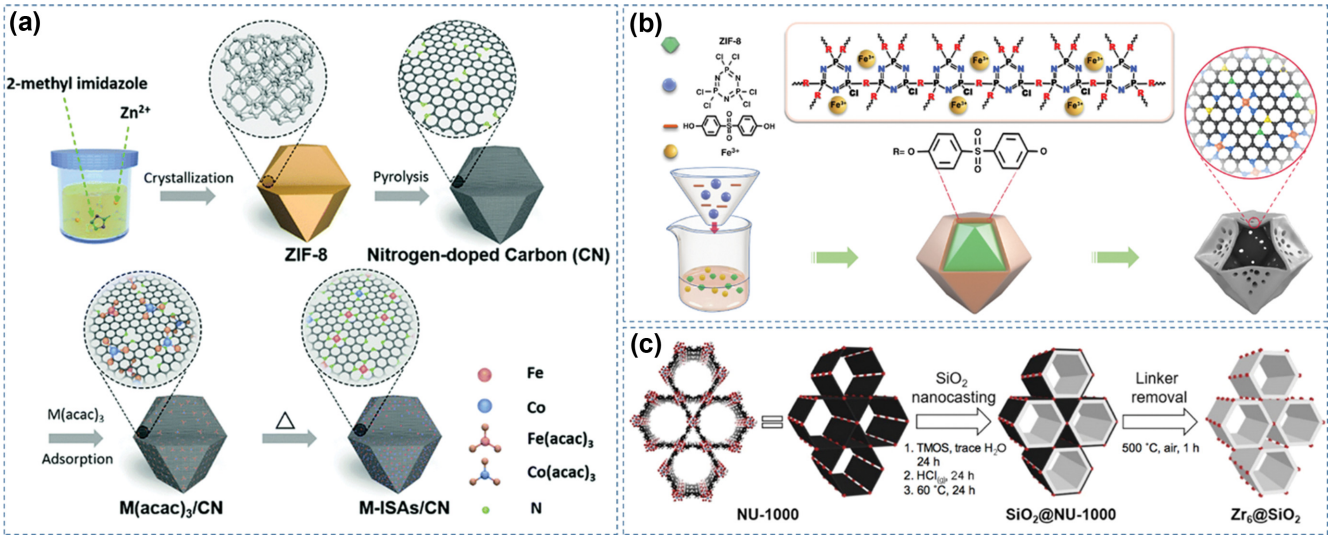

Fig. 7. Other strategies. (a) Schematic illustration for the preparation of metal SAs/NC *via* adsorption-pyrolysis strategy (Reprinted with permission from Ref. [105], Copyright 2018, Royal Chemical Society), (b) Schematic illustration for the preparation of single iron atomic sites supported on a nitrogen, phosphorus and sulfur co-doped hollow carbon polyhedron (Fe-SAs/NPS-HC) *via* polymer-assisted pyrolysis, (Licensed under CC-BY from Ref. [84]), (c) Schematic illustration for the process of stabilizing the oxozirconium clusters in NU-1000 by nanocasting with silica, (Reprinted with permission from Ref. [87], Copyright 2016, American Chemical Society).

The SiO_2 protective layer can be also introduced either into the MOFs [85,87] or onto the surface of MOFs [110,111] before pyrolysis to suppress the particle migration and sintering. The SiO_2 layer provides additional protection by creating thermally stable metal atoms/SiO_2 interfaces, affording Fe-NC SACs with high Fe loading (3.46 wt%) [85]. On the other hand, Stein and coworkers proposed thermal stabilization of MOF-derived single-site clusters through silica nanocasting (Fig. 7(c)). Previously, the nanocasting approach has been widely used for synthesis of mesoporous materials with inverse replica structure of the parent templates [128-130]. Instead, Stein's group used nanocasted-silica as a thermally stable scaffold anchoring the oxozirconium clusters in NU-1000 [87]. Silica precursor (tetramethylorthosilicate) was infiltrated into the pores of NU-1000, and then condensed together *via* vapor-phase HCl treatment, thereby resulting in formation of thin silica layer. During calcination under air at 500-600 °C, organic linkers thermally decomposed while oxozirconium clusters were kept embedded/isolated in a silica matrix (namely, Zr_6@SiO_2). The catalytically active atomic Zn species is highly concentrated and well dispersed on a thermally stable silica support.

CONCLUSION AND FUTURE PERSPECTIVE

MOF-derived SACs have shown great promise to become ideal catalysts that bridge the gap between heterogeneous and homogeneous catalysts. Controlled pyrolysis of predesigned MOFs leads to formation of metal SA/support materials. MOF-derived SACs often inherit the uniform particle morphology, high porosity and high surface area of parent MOFs, which are beneficial for increasing the mass transport capability and the accessibility to active sites. In addition, MOF-derived SACs usually exhibit higher electronic conductivity and thermal stability than MOF-supported SACs, so they can be utilized in a wide range of catalytic processes where MOF-supported SACs are not available. Although remarkable progress has been made in the fabrication of MOF-derived SACs, this research field is still in its infancy with several challenges to be addressed in the future.

(i) MOF-derived SACs still suffer from low metal loading, typically less than 1.0 wt%. This significantly decreases the active site density and catalytic activity. To generate atomically dispersed metal sites, researchers have minimized the amount of metal content and enlarged the distance between metal atoms through various synthetic strategies. So far, only a few MOF-derived SACs have achieved more than 4 wt% metal loading (Table 1), which must be increased for practical application of SACs. The SMSI effect could be an effective tool to decrease the particle size of metals and to stabilize the isolated atoms on various supports. For example, N-sites are able to trap mobile metals by forming M-N bonds, so they can effectively anchor SA metals to inhibit their migration and aggregation. Indeed, very recently, Wang and coworkers reported Fe SACs with record-high-metal loading of 30.0 wt% *via* pyrolysis of coordination polymers with high N content [131]. N-rich dicyandiamide, formaldehyde, and metal salt (*e.g.*, iron nitrate) were reacted together in hot water to form Fe ion-coordinated dicyandiamide-formaldehyde resins. These metal-coordinated polymers were converted to Fe SACs after two-step calcination and reduction heat treatments. Preparation of a series of SACs with different metal centers (Fe, Ni, Cu, Zn, Ru, Rh, Pd, Pt, and Ir) was also demonstrated. Therefore, it is highly desirable to introduce large amount nitrogen species using nitrogen-rich ligands and secondary guest molecules with high nitrogen content [132].

(ii) Development of simple and scalable synthesis strategies is highly required from a practical point of view. Previous strategies usually relied on complicated multi-steps including preparation of MOFs, post-synthetic modification, pyrolysis, and acid etching. In addition, the MOF precursors and guest molecules themselves are often cost-intensive, limiting large-scale mass production of MOF-derived SACs. Thus, direct fabrication of SACs with minimum number of synthetic steps will be greatly appreciated. The use of inexpensive precursors from large-scale industrial production or earth-abundant natural minerals will be important future research topics.

(iii) Precise control over the structures from molecular- to macroscopic level is necessary. The catalytically active sites are comprised of metal atoms and neighboring heteroatoms (carbon, nitrogen and others). Thus, coordination environments, such as coordinated atom number, metal-N configuration, need to be controlled accurately as they have a significant impact on catalytic activity and selectivity [133,134]. Other than SACs, dual-atom/cluster metal catalysts have gained increasing interest in recent years as they can potentially show unique cooperative or synergistic effects that are difficult to achieve in SACs [5,27]. Each atom can act as an individual active site, and minor changes in atom number and composition can significantly affect the catalytic activity and selectivity of a reaction [135-137]. However, dual-atom/cluster catalysts with well-defined atomic configurations have not been realized yet and will be the subject of future research. On the other hand, the mesoscopic pore size, structure and macroscopic particle morphology should be controlled to increase the accessibility to active SA sites and the mass transport capability. To this end, hierarchically porous structures with well-defined 3D networks would be highly attractive, ensuring rapid mass transfer and efficient utilization of active sites. Hybridization of MOF with other substrates such as carbon nanotubes, graphene, covalent-organic framework is also suggested [36,138-140].

(iv) Detailed formation mechanism of MOF-derived SACs still remains largely unexplored. The physicochemical properties of MOF-derived materials themselves are highly dependent on the pyrolysis condition, such as temperature, ramping rate, retention time and gas atmosphere, as well as the incorporation of guest species [36]. Therefore, it is highly recommended to investigate the underlying thermal transformation mechanisms to prepare MOF-derived SACs with desired properties (*e.g.*, heteroatom content, surface area, porosity, degree of graphitization, and degree of particle aggregation). Various *in situ* characterization techniques such as *in situ* X-ray absorption spectroscopy and *in situ* TEM will provide new insights into the formation mechanisms of MOF-derived SACs.

ACKNOWLEDGEMENTS

This work was supported by the National Research Foundation of Korea (NRF) grant funded by the Korea government (MSIT)

(No. 2020R1F1A1065283) and by C1 Gas Refinery Program through the NRF funded by the Ministry of Science, ICT and Future Planning (2015M3D3A1A01064899).

REFERENCES

1. J. Hagen, *Industrial catalysis: a practical approach*, John Wiley & Sons, Hoboken (2015).
2. A. Bavykina, N. Kolobov, I. S. Khan, J. A. Bau, A. Ramirez and J. Gascon, *Chem. Rev.*, **120**, 8468 (2020).
3. S. Mitchell, E. Vorobyeva and J. Pérez-Ramírez, *Angew. Chem. Int. Ed.*, **57**, 15316 (2018).
4. J. K. Nørskov, F. Studt, F. Abild-Pedersen and T. Bligaard, *Fundamental concepts in heterogeneous catalysis*, John Wiley & Sons, Hoboken (2014).
5. C.-C. Hou, H.-F. Wang, C. Li and Q. Xu, *Energy Environ. Sci.*, **13**, 1658 (2020).
6. J. Wang, Z. Li, Y. Wu and Y. Li, *Adv. Mater.*, **30**, 1801649 (2018).
7. H. Fei, J. Dong, D. Chen, T. Hu, X. Duan, I. Shakir, Y. Huang and X. Duan, *Chem. Soc. Rev.*, **48**, 5207 (2019).
8. M. J. Hülsey, J. Zhang and N. Yan, *Adv. Mater.*, **30**, 1802304 (2018).
9. X. Cui, W. Li, P. Ryabchuk, K. Junge and M. Beller, *Nat. Catal.*, **1**, 385 (2018).
10. A. Wang, J. Li and T. Zhang, *Nat. Rev. Chem.*, **2**, 65 (2018).
11. S. Yang, J. Kim, Y. J. Tak, A. Soon and H. Lee, *Angew. Chem. Int. Ed.*, **55**, 2058 (2016).
12. B. Qiao, A. Wang, X. Yang, L. F. Allard, Z. Jiang, Y. Cui, J. Liu, J. Li and T. Zhang, *Nat. Chem.*, **3**, 634 (2011).
13. Z. Song, L. Zhang, K. Doyle-Davis, X. Fu, J. L. Luo and X. Sun, *Adv. Energy Mater.*, **10**, 2001561 (2020).
14. A. Han, B. Wang, A. Kumar, Y. Qin, J. Jin, X. Wang, C. Yang, B. Dong, Y. Jia and J. Liu, *Small Mtd.*, **3**, 1800471 (2019).
15. Y.-S. Wei, M. Zhang, R. Zou and Q. Xu, *Chem. Rev.*, **120**, 12089 (2020).
16. N. Zhang, C. Ye, H. Yan, L. Li, H. He, D. Wang and Y. Li, *Nano Res.*, **13**, 3165 (2020).
17. Z. Liang, C. Qu, D. Xia, R. Zou and Q. Xu, *Angew. Chem. Int. Ed.*, **57**, 9604 (2018).
18. D. Li, H.-Q. Xu, L. Jiao and H.-L. Jiang, *EnergyChem*, **1**, 100005 (2019).
19. X. Li and Q.-L. Zhu, *EnergyChem*, **2**, 100033 (2020).
20. X. Li, S. Zheng, L. Jin, Y. Li, P. Geng, H. Xue, H. Pang and Q. Xu, *Adv. Energy Mater.*, **8**, 1800716 (2018).
21. Z. Liang, R. Zhao, T. Qiu, R. Zou and Q. Xu, *EnergyChem*, **1**, 100001 (2019).
22. M. Liu, L. Wang, K. Zhao, S. Shi, Q. Shao, L. Zhang, X. Sun, Y. Zhao and J. Zhang, *Energy Environ. Sci.*, **12**, 2890 (2019).
23. T. Sun, L. Xu, D. Wang and Y. Li, *Nano Res.*, **12**, 2067 (2019).
24. Z. Song, L. Zhang, K. Doyle-Davis, X. Fu, J.-L. Luo and X. Sun, *Adv. Energy Mater.*, **10**, 2001561 (2020).
25. C. Lu, R. Fang and X. Chen, *Adv. Mater.*, **32**, 1906548 (2020).
26. Z. Zhuang, Q. Kang, D. Wang and Y. Li, *Nano Res.*, **13**, 1856 (2020).
27. D.-D. Ma and Q.-L. Zhu, *Coord. Chem. Rev.*, **422**, 213483 (2020).
28. C. Cao, D.-D. Ma, J.-F. Gu, X. Xie, G. Zeng, X. Li, S.-G. Han, Q.-L. Zhu, X.-T. Wu and Q. Xu, *Angew. Chem. Int. Ed.*, **59**, 15014 (2020).
29. S.-G. Han, D.-D. Ma, S.-H. Zhou, K. Zhang, W.-B. Wei, Y. Du, X.-T. Wu, Q. Xu, R. Zou and Q.-L. Zhu, *Appl. Catal. B: Environ.*, **283**, 119591 (2020).
30. S. Youk, J. Hwang, S. Lee, M. S. Kim and J. Lee, *Small Methods*, **3**, 1800293 (2019).
31. L. Lin, W. Zhou, R. Gao, S. Yao, X. Zhang, W. Xu, S. Zheng, Z. Jiang, Q. Yu and Y.-W. Li, *Nature*, **544**, 80 (2017).
32. H. Yan, H. Cheng, H. Yi, Y. Lin, T. Yao, C. Wang, J. Li, S. Wei and J. Lu, *J. Am. Chem. Soc.*, **137**, 10484 (2015).
33. J. Jones, H. Xiong, A. T. DeLaRiva, E. J. Peterson, H. Pham, S. R. Challa, G. Qi, S. Oh, M. H. Wiebenga and X. I. P. Hernández, *Science*, **353**, 150 (2016).
34. H. Furukawa, K. E. Cordova, M. O'Keeffe and O. M. Yaghi, *Science*, **341**, 1230444 (2013).
35. O. M. Yaghi, M. O'keeffe, N. W. Ockwig, H. K. Chae, M. Eddaoudi and J. Kim, *Nature*, **423**, 705 (2003).
36. J. Hwang, A. Ejsmont, R. Freund, J. Goscianska, B. V. K. J. Schmidt and S. Wuttke, *Chem. Soc. Rev.*, **49**, 3348 (2020).
37. J. Hwang, R. Walczak, M. Oschatz, N. V. Tarakina and B. V. K. J. Schmidt, *Small*, **15**, 1901986 (2019).
38. X. Zhang, A. Chen, M. Zhong, Z. Zhang, X. Zhang, Z. Zhou and X.-H. Bu, *Electrochem. Energy Rev.*, **2**, 29 (2019).
39. J. Hwang, R. Yan, M. Oschatz and B. V. K. J. Schmidt, *J. Mater. Chem. A*, **6**, 23521 (2018).
40. H. B. Wu and X. W. D. Lou, *Sci. Adv.*, **3**, eaap9252 (2017).
41. C. Wang, J. Kim, J. Tang, M. Kim, H. Lim, V. Malgras, J. You, Q. Xu, J. Li and Y. Yamauchi, *Chem*, **6**, 19 (2020).
42. R. R. Salunkhe, Y. V. Kaneti and Y. Yamauchi, *ACS Nano*, **11**, 5293 (2017).
43. S. Dang, Q.-L. Zhu and Q. Xu, *Nat. Rev. Mater.*, **3**, 17075 (2017).
44. L. Liu and A. Corma, *Chem. Rev.*, **118**, 4981 (2018).
45. C. Zhu, S. Fu, Q. Shi, D. Du and Y. Lin, *Angew. Chem. Int. Ed.*, **56**, 13944 (2017).
46. X.-F. Yang, A. Wang, B. Qiao, J. Li, J. Liu and T. Zhang, *Acc. Chem. Res.*, **46**, 1740 (2013).
47. Y. Chen, S. Ji, C. Chen, Q. Peng, D. Wang and Y. Li, *Joule*, **2**, 1242 (2018).
48. Y. Peng, B. Lu and S. Chen, *Adv. Mater.*, **30**, 1801995 (2018).
49. P. Yin, T. Yao, Y. Wu, L. Zheng, Y. Lin, W. Liu, H. Ju, J. Zhu, X. Hong, Z. Deng, G. Zhou, S. Wei and Y. Li, *Angew. Chem. Int. Ed.*, **55**, 10800 (2016).
50. X. Han, X. Ling, Y. Wang, T. Ma, C. Zhong, W. Hu and Y. Deng, *Angew. Chem. Int. Ed.*, **58**, 5359 (2019).
51. X. X. Wang, D. A. Cullen, Y. T. Pan, S. Hwang, M. Wang, Z. Feng, J. Wang, M. H. Engelhard, H. Zhang and Y. He, *Adv. Mater.*, **30**, 1706758 (2018).
52. X. Wang, Z. Chen, X. Zhao, T. Yao, W. Chen, R. You, C. Zhao, G. Wu, J. Wang and W. Huang, *Angew. Chem. Int. Ed.*, **57**, 1944 (2018).
53. H. Zhang, S. Hwang, M. Wang, Z. Feng, S. Karakalos, L. Luo, Z. Qiao, X. Xie, C. Wang, D. Su, Y. Shao and G. Wu, *J. Am. Chem. Soc.*, **139**, 14143 (2017).
54. S. Fu, C. Zhu, D. Su, J. Song, S. Yao, S. Feng, M. H. Engelhard, D. Du and Y. Lin, *Small*, **14**, 1703118 (2018).
55. C. Yan, H. Li, Y. Ye, H. Wu, F. Cai, R. Si, J. Xiao, S. Miao, S. Xie, F. Yang, Y. Li, G. Wang and X. Bao, *Energy Environ. Sci.*, **11**, 1204 (2018).
56. X. Dai, Z. Chen, T. Yao, L. Zheng, Y. Lin, W. Liu, H. Ju, J. Zhu, X.

Hong, S. Wei, Y. Wu and Y. Li, *Chem. Commun*., **53**, 11568 (2017).
57. Y. N. Gong, L. Jiao, Y. Qian, C. Y. Pan, L. Zheng, X. Cai, B. Liu, S. H. Yu and H. L. Jiang, *Angew. Chem. Int. Ed*., **59**, 2705 (2020).
58. Y. Yang, K. Mao, S. Gao, H. Huang, G. Xia, Z. Lin, P. Jiang, C. Wang, H. Wang and Q. Chen, *Adv. Mater*., **30**, 1801732 (2018).
59. Q. Yang, C.-C. Yang, C.-H. Lin and H.-L. Jiang, *Angew. Chem. Int. Ed*., **58**, 3511 (2019).
60. B. Xu, H. Wang, W. Wang, L. Gao, S. Li, X. Pan, H. Wang, H. Yang, X. Meng, Q. Wu, L. Zheng, S. Chen, X. Shi, K. Fan, X. Yan and H. Liu, *Angew. Chem. Int. Ed.*, **58**, 4911 (2019).
61. L. Jiao, G. Wan, R. Zhang, H. Zhou, S.-H. Yu and H.-L. Jiang, *Angew. Chem. Int. Ed*., **57**, 8525 (2018).
62. Y. Lin, P. Liu, E. Velasco, G. Yao, Z. Tian, L. Zhang and L. Chen, *Adv. Mater*., **31**, 1808193 (2019).
63. Y. Ye, F. Cai, H. Li, H. Wu, G. Wang, Y. Li, S. Miao, S. Xie, R. Si, J. Wang and X. Bao, *Nano Energy*, **38**, 281 (2017).
64. Y. Zhao, H. Zhou, W. Chen, Y. Tong, C. Zhao, Y. Lin, Z. Jiang, Q. Zhang, Z. Xue and W.-C. Cheong, *J. Am. Chem. Soc*., **141**, 10590 (2019).
65. X. Wang, W. Chen, L. Zhang, T. Yao, W. Liu, Y. Lin, H. Ju, J. Dong, L. Zheng, W. Yan, X. Zheng, Z. Li, X. Wang, J. Yang, D. He, Y. Wang, Z. Deng, Y. Wu and Y. Li, *J. Am. Chem. Soc*., **139**, 9419 (2017).
66. W. Chen, J. Pei, C. T. He, J. Wan, H. Ren, Y. Wang, J. Dong, K. Wu, W. C. Cheong and J. Mao, *Adv. Mater*., **30**, 1800396 (2018).
67. Y. Chen, S. Ji, Y. Wang, J. Dong, W. Chen, Z. Li, R. Shen, L. Zheng, Z. Zhuang and D. Wang, *Angew. Chem. Int. Ed*., **56**, 6937 (2017).
68. R. Jiang, L. Li, T. Sheng, G. Hu, Y. Chen and L. Wang, *J. Am. Chem. Soc*., **140**, 11594 (2018).
69. Y. Wang, M. Wang, Z. Zhang, Q. Wang, Z. Jiang, M. Lucero, X. Zhang, X. Li, M. Gu and Z. Feng, *ACS Catal*., **9**, 6252 (2019).
70. J. Wang, G. Han, L. Wang, L. Du, G. Chen, Y. Gao, Y. Ma, C. Du, X. Cheng and P. Zuo, *Small*, **14**, 1704282 (2018).
71. Q.-L. Zhu, W. Xia, L.-R. Zheng, R. Zou, Z. Liu and Q. Xu, *ACS Energy Lett*., **2**, 504 (2017).
72. Q. Lai, L. Zheng, Y. Liang, J. He, J. Zhao and J. Chen, *ACS Catal*., **7**, 1655 (2017).
73. E. Luo, H. Zhang, X. Wang, L. Gao, L. Gong, T. Zhao, Z. Jin, J. Ge, Z. Jiang, C. Liu and W. Xing, *Angew. Chem. Int. Ed*., **58**, 12469 (2019).
74. M. Xiao, J. Zhu, G. Li, N. Li, S. Li, Z. P. Cano, L. Ma, P. Cui, P. Xu, G. Jiang, H. Jin, S. Wang, T. Wu, J. Lu, A. Yu, D. Su and Z. Chen, *Angew. Chem. Int. Ed*., **58**, 9640 (2019).
75. M. Xiao, L. Gao, Y. Wang, X. Wang, J. Zhu, Z. Jin, C. Liu, H. Chen, G. Li, J. Ge, Q. He, Z. Wu, Z. Chen and W. Xing, *J. Am. Chem. Soc*., **141**, 19800 (2019).
76. E. Zhang, T. Wang, K. Yu, J. Liu, W. Chen, A. Li, H. Rong, R. Lin, S. Ji, X. Zheng, Y. Wang, L. Zheng, C. Chen, D. Wang, J. Zhang and Y. Li, *J. Am. Chem. Soc*., **141**, 16569 (2019).
77. Y. Qu, Z. Li, W. Chen, Y. Lin, T. Yuan, Z. Yang, C. Zhao, J. Wang, C. Zhao and X. Wang, *Nat. Catal*., **1**, 781 (2018).
78. Z. Yang, B. Chen, W. Chen, Y. Qu, F. Zhou, C. Zhao, Q. Xu, Q. Zhang, X. Duan and Y. Wu, *Nat. Commun*., **10**, 1 (2019).
79. C. Zhao, C. Xiong, X. Liu, M. Qiao, Z. Li, T. Yuan, J. Wang, Y. Qu, X. Wang and F. Zhou, *Chem. Commun*., **55**, 2285 (2019).
80. Y. Deng, B. Chi, J. Li, G. Wang, L. Zheng, X. Shi, Z. Cui, L. Du, S. Liao, K. Zang, J. Luo, Y. Hu and X. Sun, *Adv. Energy Mater*., **9**, 1802856 (2019).
81. J. Yang, Z. Qiu, C. Zhao, W. Wei, W. Chen, Z. Li, Y. Qu, J. Dong, J. Luo, Z. Li and Y. Wu, *Angew. Chem. Int. Ed*., **57**, 14095 (2018).
82. S. Wei, A. Li, J.-C. Liu, Z. Li, W. Chen, Y. Gong, Q. Zhang, W.-C. Cheong, Y. Wang and L. Zheng, *Nat. Nanotech*., **13**, 856 (2018).
83. Y. He, S. Hwang, D. A. Cullen, M. A. Uddin, L. Langhorst, B. Li, S. Karakalos, A. J. Kropf, E. C. Wegener and J. Sokolowski, *Energy Environ. Sci.*, **12**, 250 (2019).
84. Y. Chen, S. Ji, S. Zhao, W. Chen, J. Dong, W.-C. Cheong, R. Shen, X. Wen, L. Zheng and A. I. Rykov, *Nat. Commun*., **9**, 1 (2018).
85. L. Jiao, R. Zhang, G. Wan, W. Yang, X. Wan, H. Zhou, J. Shui, S.-H. Yu and H.-L. Jiang, *Nat. Commun*., **11**, 2831 (2020).
86. J. Li, M. Chen, D. A. Cullen, S. Hwang, M. Wang, B. Li, K. Liu, S. Karakalos, M. Lucero, H. Zhang, C. Lei, H. Xu, G. E. Sterbinsky, Z. Feng, D. Su, K. L. More, G. Wang, Z. Wang and G. Wu, *Nat. Catal*., **1**, 935 (2018).
87. C. D. Malonzo, S. M. Shaker, L. Ren, S. D. Prinslow, A. E. Platero-Prats, L. C. Gallington, J. Borycz, A. B. Thompson, T. C. Wang, O. K. Farha, J. T. Hupp, C. C. Lu, K. W. Chapman, J. C. Myers, R. L. Penn, L. Gagliardi, M. Tsapatsis and A. Stein, *J. Am. Chem. Soc*., **138**, 2739 (2016).
88. L. Fan, P. F. Liu, X. Yan, L. Gu, Z. Z. Yang, H. G. Yang, S. Qiu and X. Yao, *Nat. Commun*., **7**, 1 (2016).
89. Y.-Z. Chen, C. Wang, Z.-Y. Wu, Y. Xiong, Q. Xu, S.-H. Yu and H.-L. Jiang, *Adv. Mater*., **27**, 5010 (2015).
90. R. C. Klet, T. C. Wang, L. E. Fernandez, D. G. Truhlar, J. T. Hupp and O. K. Farha, *Chem. Mater.*, **28**, 1213 (2016).
91. X. Chen, D.-D. Ma, B. Chen, K. Zhang, R. Zou, X.-T. Wu and Q.-L. Zhu, *Appl. Catal. B: Environ*., **267**, 118720 (2020).
92. F. Xiao, G.-L. Xu, C.-J. Sun, M. Xu, W. Wen, Q. Wang, M. Gu, S. Zhu, Y. Li, Z. Wei, X. Pan, J. Wang, K. Amine and M. Shao, *Nano Energy*, **61**, 60 (2019).
93. Q. Liu, X. Liu, L. Zheng and J. Shui, *Angew. Chem. Int. Ed*., **57**, 1204 (2018).
94. C. Zhao, X. Dai, T. Yao, W. Chen, X. Wang, J. Wang, J. Yang, S. Wei, Y. Wu and Y. Li, *J. Am. Chem. Soc*., **139**, 8078 (2017).
95. Q. Liu, Y. Li, L. Zheng, J. Shang, X. Liu, R. Yu and J. Shui, *Adv. Energy Mater*., **10**, 2000689 (2020).
96. Z. Geng, Y. Liu, X. Kong, P. Li, K. Li, Z. Liu, J. Du, M. Shu, R. Si and J. Zeng, *Adv. Mater*., **30**, 1803498 (2018).
97. Y. Xiong, J. Dong, Z.-Q. Huang, P. Xin, W. Chen, Y. Wang, Z. Li, Z. Jin, W. Xing and Z. Zhuang, *Nat. Nanotech*., **15**, 390 (2020).
98. J. Han, X. Meng, L. Lu, J. Bian, Z. Li and C. Sun, *Adv. Funct. Mater*., **29**, 1808872 (2019).
99. Q.-L. Zhu and Q. Xu, Chem, **1**, 220 (2016).
100. Q.-L. Zhu, J. Li and Q. Xu, *J. Am. Chem. Soc*., **135**, 10210 (2013).
101. L. Wang, L. Wang, X. Meng and F.-S. Xiao, *Adv. Mater*., **31**, 1901905 (2019).
102. Y. Dai, P. Lu, Z. Cao, C. T. Campbell and Y. Xia, *Chem. Soc. Rev*., **47**, 4314 (2018).
103. Y. Qu, B. Chen, Z. Li, X. Duan, L. Wang, Y. Lin, T. Yuan, F. Zhou, Y. Hu and Z. Yang, *J. Am. Chem. Soc*., **141**, 4505 (2019).
104. J. Li, L. Jiao, E. Wegener, L. L. Richard, E. Liu, A. Zitolo, M. T. Sougrati, S. Mukerjee, Z. Zhao and Y. Huang, *J. Am. Chem. Soc*., **142**, 1417 (2019).
105. D. Zhang, W. Chen, Z. Li, Y. Chen, L. Zheng, Y. Gong, Q. Li, R. Shen, Y. Han, W.-C. Cheong, L. Gu and Y. Li, *Chem. Commun*.,

54, 4274 (2018).
106. J. Li, P. Pršlja, T. Shinagawa, A. J. Martín Fernández, F. Krumeich, K. Artyushkova, P. Atanassov, A. Zitolo, Y. Zhou, R. García-Muelas, N. López, J. Pérez-Ramírez and F. Jaouen, *ACS Catal.*, **9**, 10426 (2019).
107. S. H. Ahn, M. J. Klein and A. Manthiram, *Adv. Energy Mater.*, **7**, 1601979 (2017).
108. T. Al-Zoubi, Y. Zhou, X. Yin, B. Janicek, C. Sun, C. E. Schulz, X. Zhang, A. A. Gewirth, P. Huang, P. Zelenay and H. Yang, *J. Am. Chem. Soc.*, **142**, 5477 (2020).
109. H. Yang, Q. Lin, C. Zhang, X. Yu, Z. Cheng, G. Li, Q. Hu, X. Ren, Q. Zhang and J. Liu, *Nat. Commun.*, **11**, 1 (2020).
110. L. Shang, H. Yu, X. Huang, T. Bian, R. Shi, Y. Zhao, G. I. Waterhouse, L. Z. Wu, C. H. Tung and T. Zhang, *Adv. Mater.*, **28**, 1668 (2016).
111. X. Wan, X. Liu, Y. Li, R. Yu, L. Zheng, W. Yan, H. Wang, M. Xu and J. Shui, *Nat. Catal.*, **2**, 259 (2019).
112. Q. Li, W. Chen, H. Xiao, Y. Gong, Z. Li, L. Zheng, X. Zheng, W. Yan, W. C. Cheong and R. Shen, *Adv. Mater.*, **30**, 1800588 (2018).
113. A. Han, W. Chen, S. Zhang, M. Zhang, Y. Han, J. Zhang, S. Ji, L. Zheng, Y. Wang and L. Gu, *Adv. Mater.*, **30**, 1706508 (2018).
114. Y. He, S. Hwang, D. A. Cullen, M. A. Uddin, L. Langhorst, B. Li, S. Karakalos, A. J. Kropf, E. C. Wegener, J. Sokolowski, M. Chen, D. Myers, D. Su, K. L. More, G. Wang, S. Litster and G. Wu, *Energy Environ. Sci.*, **12**, 250 (2019).
115. S. Kim, J. Hwang, J. Lee and J. Lee, *Sci. Adv.*, **6**, eabb3814 (2020).
116. S. Kim, M. Ju, J. Lee, J. Hwang and J. Lee, *J. Am. Chem. Soc.*, **142**, 9250 (2020).
117. J. Hwang, S. Kim, U. Wiesner and J. Lee, *Adv. Mater.*, **30**, 1801127 (2018).
118. S. Kim, I. Jeong, J. Hwang, M. J. Ko and J. Lee, *Chem. Commun.*, **53**, 4100 (2017).
119. J. Hwang, C. Jo, K. Hur, J. Lim, S. Kim and J. Lee, *J. Am. Chem. Soc.*, **136**, 16066 (2014).
120. C. Jo, J. Hwang, W.-G. Lim, J. Lim, K. Hur and J. Lee, *Adv. Mater.*, **30**, 1703829 (2018).
121. J. Hwang, C. Jo, M. G. Kim, J. Chun, E. Lim, S. Kim, S. Jeong, Y. Kim and J. Lee, *ACS Nano*, **9**, 5299 (2015).
122. J. Hwang, S. H. Woo, J. Shim, C. Jo, K. T. Lee and J. Lee, *ACS Nano*, **7**, 1036 (2013).
123. M. Kalaj, K. C. Bentz, S. Ayala, J. M. Palomba, K. S. Barcus, Y. Katayama and S. M. Cohen, *Chem. Rev.*, **120**, 8267 (2020).
124. T. Kitao, Y. Zhang, S. Kitagawa, B. Wang and T. Uemura, *Chem. Soc. Rev.*, **46**, 3108 (2017).
125. J. Hwang, H.-C. Lee, M. Antonietti and B. V. K. J. Schmidt, *Polym. Chem.*, **8**, 6204 (2017).
126. J. Hwang, T. Heil, M. Antonietti and B. V. K. J. Schmidt, *J. Am. Chem. Soc.*, **140**, 2947 (2018).
127. H.-C. Lee, J. Hwang, U. Schilde, M. Antonietti, K. Matyjaszewski and B. V. K. J. Schmidt, *Chem. Mater.*, **30**, 2983 (2018).
128. D. Gu and F. Schüth, *Chem. Soc. Rev.*, **43**, 313 (2014).
129. K.-S. Ha, G. Kwak, K.-W. Jun, J. Hwang and J. Lee, *Chem. Commun.*, **49**, 5141 (2013).
130. I. Jeong, C. Jo, A. Anthonysamy, J.-M. Kim, E. Kang, J. Hwang, E. Ramasamy, S.-W. Rhee, J. K. Kim, K.-S. Ha, K.-W. Jun and J. Lee, *ChemSusChem*, **6**, 299 (2013).
131. Y. Xiong, W. Sun, P. Xin, W. Chen, X. Zheng, W. Yan, L. Zheng, J. Dong, J. Zhang, D. Wang and Y. Li, *Adv. Mater.*, **32**, 2000896 (2020).
132. D. Liu, C. Wu, S. Chen, S. Ding, Y. Xie, C. Wang, T. Wang, Y. A. Haleem, Z. ur Rehman and Y. Sang, *Nano Res.*, **11**, 2217 (2018).
133. J. Yang, W. Li, D. Wang and Y. Li, *Adv. Mater.*, **32**, 2003300 (2020).
134. T. Sun, S. Mitchell, J. Li, P. Lyu, X. Wu, J. Pérez-Ramírez and J. Lu, *Adv. Mater.*, **33**, 2003075 (2021).
135. E. C. Tyo and S. Vajda, *Nat. Nanotech.*, **10**, 577 (2015).
136. R. Zhao, Z. Liang, S. Gao, C. Yang, B. Zhu, J. Zhao, C. Qu, R. Zou and Q. Xu, *Angew. Chem. Int. Ed.*, **58**, 1975 (2019).
137. L. Zhang, J. M. T. A. Fischer, Y. Jia, X. Yan, W. Xu, X. Wang, J. Chen, D. Yang, H. Liu and L. Zhuang, *J. Am. Chem. Soc.*, **140**, 10757 (2018).
138. Y. Lu, J. Zhang, W. Wei, D.-D. Ma, X.-T. Wu and Q.-L. Zhu, *ACS Appl. Mater. Interfaces*, **12**, 37986 (2020).
139. Y. Zheng, S. Zheng, H. Xue and H. Pang, *Adv. Funct. Mater.*, **28**, 1804950 (2018).
140. S. M. J. Rogge, A. Bavykina, J. Hajek, H. Garcia, A. I. Olivos-Suarez, A. Sepúlveda-Escribano, A. Vimont, G. Clet, P. Bazin and F. Kapteijn, *Chem. Soc. Rev.*, **46**, 3134 (2017).

Jongkook Hwang received his Ph.D. in department of chemical engineering from Pohang University of Science and Technology (POSTECH) in 2016. After his first post-doctoral training at Max Planck Institute of Colloids and Interfaces, he moved to Utrecht University where he worked on development of heterogeneous catalysts for preferential CO oxidation in H_2. In 2020, he was appointed as an assistant professor in department of chemical engineering at Ajou University, Korea. His research interest is synthesis of nanoporous materials with well-defined structures and morphologies for energy- and catalytic applications.